JOURNAL OF MATERIALS SCIENCE 26 (1991) 5888–5898

Constituent scale and property effects on fibre–matrix debonding and pull-out

V. M. KARBHARI, D. J. WILKINS
Center for Composite Materials, University of Delaware, Newark, DE 19716, USA

An improved formulation for the pull-out problem is presented, that accounts for mechanical equilibrium at the embedded fibre end, and frictional interfacial forces in the debonded portion. The externally applied stress required to cause catastrophic pull-out is determined as a function of various parameters including the ratio of interfacial shear strength to the interfacial frictional stress. The effects of fibril bundles on stress transfer and initiation of debonding is also investigated and results are compared with those for single fibres. A comparison is made between the stress needed to cause intermediate non-catastrophic debonding with that needed for catastrophic debonding and subsequent pull-out. Some new results are presented which explain phenomenon from earlier experimental investigations, and which show the importance of the constituent scaling on the micromechanisms of damage under consideration.

1. Introduction

Unlike polycrystalline solids which show a specified mode of fracture, a composite is subject to diverse micromechanisms of damage, any one of which may by itself, or in conjunction with others, cause the ultimate failure of the material. Some of these mechanisms contribute to the toughness of the fibrous composite and, if we are to fully utilize the properties of these advanced materials it is essential that we not only understand the mechanics of each mechanism of damage, but also the effect of constituent scaling and interaction on the macro-response of the material. Fracture toughness of composites is a result of various toughening mechanisms such as fibre–matrix debonding and subsequent pull-out. Under monotonic loading on a composite small cracks form in the matrix normal to the direction of loading. This is specially seen in unidirectional composites loaded in the direction of the fibrous reinforcement. This causes the transfer of load to the fibres with increasing shear stress, eventually causing the failure of the bond between the fibre and the surrounding matrix. The cylindrical crack at the interface propagates from the initial matrix crack causing debonding along the fibre [1]. Fibre strength is dependent on its length and diameter, and fibres break at their weakest points, not necessarily along the matrix crack plane. The length of the fibre that protrudes from the crack plane after composite failure is known as the pull-out length.

The tailoring of composites for toughness is dictated to a large extent by the properties of the interface/interphase [2]. The fibre–matrix debond problem thus assumes critical importance to the design of tough composites. Although the debonding problem has received considerable attention, it has yet to be completely characterized and understood. Most of the work has been concentrated towards the evaluation of the bonding strength or the contribution to fracture toughness due to pull-out, without an in-depth investigation into the effects of constituent scale (fibre diameter and embedded length, bundle size, fibre packing, fibre volume fraction) and elastic properties of the constituents. Knowledge of this is expected to be useful in controlling the fracture mechanisms and their sequence, as well as in tailoring composites through scale [3]. Previous investigations can be classified into two classes. The first comprises a set of approaches based on a maximum shear stress criterion [4–7], whereas the second uses a fracture mechanics approach [8–13]. Statistical aspects of pull-out have been discussed in terms of the variation in fibre strength [14, 15].

Gray [16] reviewed a number of theories and experiments and stressed that it was important to consider both the interfacial shear stresses due to elastic bonding and the frictional resistance due to slippage. The interfacial shear stress is overcome by the debonding of the fibre–matrix interface. However, frictional stresses still exist due to resin shrinkage during processing, or from the mismatch of expansion coefficients during cooling, and from the Poisson's contraction of the fibre loaded in tension. This influence has largely been neglected except in a few investigations [5–7, 9], from which only the formulation of Gao *et al.* [9] includes these effects explicitly.

In model pull-out experiments, a single fibre is embedded in matrix, and a load is applied to the system to induce debonding and subsequent pull-out. The most common form follows the procedure of Takaku and Arridge [7] or a modification thereof, wherein the wire end is clamped to a load cell and the resin block clamped to the crosshead using minimum pressure. The block is then displaced at a constant rate. Numerous variations of this exist, including tests

0022–2461/91 $03.00 + .12

which try to duplicate the formation of a matrix crack in a composite, normal to the fibre cross section, with the use of a Teflon sheet.

It must be kept in mind that in order to truly tailor composites through the control of mechanisms such as debonding and pull-out, the creation of an appropriate interphase is essential. The interphase is the region responsible for transmitting the interaction between the fibre and matrix [17] within which region the two constituent phases are combined so as to be indistinct. The interface, however, as is used in the theories mentioned above, and in the formulation following, is only a two dimensional border separating the two phases of fibre and matrix. Thus, the theories are at best, approximations, as they do not consider the effect of the interphase, which is responsible for the synergism between the matrix and the reinforcement.

The objectives of this paper are to investigate the effects of constituent scale and relative properties on the mechanisms of debonding and pull-out using a shear-lag approach.

2. Formulation

In order to analyse the fibre–matrix debond problem in the context of fibre debonding and subsequent pull-out, consider the composite cylinder shear-lag model, as in Fig. 1, wherein a single fibre of radius, a, and embedded length, l, is encased within a matrix co-axial cylinder of radius, b. Clearly the system models a representative volume of a uniaxially reinforced composite with a fibre volume fraction V_f as represented by the area function of fibres in a plane vertical to the cylinder, such that $(a/b)^2 = V_f$. It is assumed however that the stress field is not affected by the interaction between fibres in adjacent cylinders, and that the fibre and matrix are perfectly bonded, and behave elastically. The configuration in Fig. 1 depicts a fibre of embedded length, l, with the matrix crack plane normal to the fibre. The origin of the system is taken to be at the embedded end of the fibre. The fibre is subjected to a uniaxial external stress, σ_0, and an interfacial stress, τ. At the outset it is assumed that there is no slip between the fibre and the matrix in $0 \leq z \leq l$, i.e a case of perfect bonding.

The constitutive equations governing stress transfer can be derived using the shear-lag approach, similar to that used in [5, 18]. The shear stress within the matrix region is expressed as

$$\tau_m = G_m \frac{dw_m}{dr} \tag{1}$$

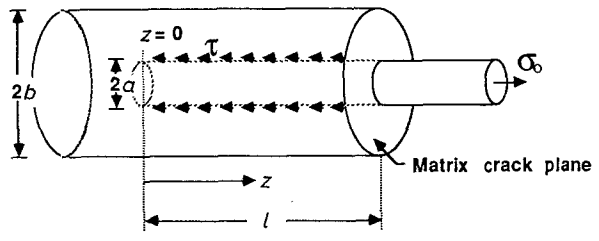

Figure 1 Schematic of the shear-lag model.

where G_m is the shear modulus of the matrix and w_m is the axial displacement of the matrix. The stress distribution is one of circular symmetry with both matrix displacement and shear stress varying as a function of the radial distance, r, from the fibre axis. Equating shear stresses within the matrix and at the fibre–matrix interface, τ

$$a\tau = r\tau_m \tag{2}$$

Integrating the expression for the interfacial shear stress obtained by substituting Equation 2 in Equation 1

$$\int_a^b \frac{a}{r}\tau\,dr = \int_{w_a}^{w_b} \frac{E_m}{2(1+\nu_m)}\,dw_m$$
$$\tau = \frac{(w_b - w_a)E_m}{2a(1+\nu_m)\ln(b/a)} \tag{3}$$

and,

$$\tau_m = \frac{(w_b - w_a)E_m}{2r(1+\nu_m)\ln(b/a)} \tag{4}$$

where E_m and ν_m are the Young's modulus and Poisson's ratio of the matrix, and w_m and w_a are the matrix axial displacement at $r = b$ and fibre displacement at $r = a$, respectively. It is assumed that the fibre displacement does not vary with radial distance.

So far we have considered only a single fibre surrounded by matrix. We can generalize this to include the effect of fibre packing through the term b/a [19]. Consider hexagonal packing as in Fig. 2. The area of the matrix within the triangular region is $3^{\frac{1}{2}}b^2/4$, whereas the area of fibres included within is $\pi a^2/2$.

$$V_f = \frac{\pi a^2}{2}\frac{4}{3^{\frac{1}{2}}b^2} = \frac{2\pi a^2}{3^{\frac{1}{2}}b^2}$$
$$\text{i.e.,}\ \frac{b}{a} = \left\{\frac{2\pi}{3^{\frac{1}{2}}V_f}\right\}^{1/2}$$

Similarly, for a square packing arrangement $b/a = \{\pi/V_f\}^{1/2}$. Representing the packing factor by P, we may write

$$\frac{b}{a} = \left\{\frac{P}{V_f}\right\}^{1/2} \tag{5}$$

If $P = 1$, we are simply considering the cylinder model (Fig. 1) without any correction for fibre packing.

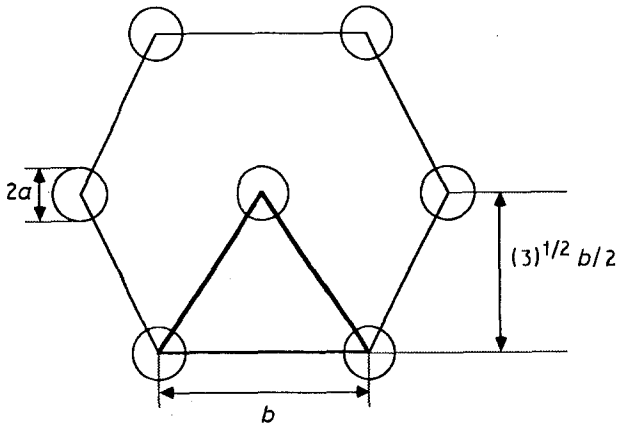

Figure 2 Hexagonal packing arrangement.

The axial stress in a constituent, σ_α, can be related to the axial displacement, w_α, where α represents either a matrix or fibre element by

$$\sigma_\alpha = E_\alpha \frac{dw_\alpha}{dz} \tag{6}$$

Substitution of Equation 1 in Equation 4, followed by integration, and the use of Equation 6 leads to an expression for the matrix stress as

$$\sigma_m = \varepsilon\sigma_f + (\sigma_b - \varepsilon\sigma_f)\frac{\ln(r/a)}{\ln(b/a)} \tag{7}$$

where $\varepsilon = E_m/E_f$, and $\sigma_b = E_m dw_b/dz$ is the axial stress in a matrix element at the outer edge of the cylinder ($r = b$) which represents the matrix stress at a radial distance from the centre of the fibre at which displacement in the matrix is equal to the average displacement in the matrix. Substitution of Equation 7 in an expression for equilibrium of stresses in constituents

$$\sigma_f + \frac{2}{a}\int_a^b r\sigma_m dr = \sigma_0 \tag{8}$$

leads to the evaluation of the matrix stress at an element equidistant from the two fibres as

$$\sigma_b = \frac{\left\{a^2\sigma_0 + \sigma_f\left[\left(a^2 - \frac{b^2 - a^2)}{2\ln(b/a)}\right)\varepsilon - a^2\right]\right\}}{\left[b^2 - \frac{b^2 - a^2}{2\ln(b/a)}\right]} \tag{9}$$

For shear forces to be in equilibrium with the tensile forces in the fibre

$$\frac{d\sigma_f}{dz} = -\frac{2\tau}{a} \tag{10}$$

Substituting Equation 3, differentiating with respect to the axial coordinate, z, and using Equations 6 and 7, the resulting differential equation may be written in the form

$$\frac{d^2\sigma_f}{dz^2} = m^2\left[\sigma_f - \frac{\sigma_0}{1 + \Phi\varepsilon}\right] \tag{11}$$

where

$$m = \left\{\frac{1 + \Phi\varepsilon}{(1 + \nu_m)\left[b^2\ln(b/a) - \frac{b^2 - a^2}{2}\right]}\right\}^{1/2} \tag{12}$$

and,

$$\Phi = \left(\frac{b^2}{a^2} - 1\right)$$

Previous solutions for stress transfer have been mostly limited to the case of the embedded fibre end being debonded from the matrix [6, 20, 21]. However, it is possible that at least initially, the embedded end would be bonded. Stress transfer at the end was modelled using a finite difference technique [22, 23] and was shown to account for greater than 25% of the maximum fibre strain. The importance of the assumption of adhesion across the end has been demonstrated using finite element approaches [24–27], but since the investigations used only small systems, the importance of finite size was not thoroughly assessed. Analytical solutions for the bonded case were not modelled till recently [5, 18, 28]. In the context of this study, two cases are considered as defined below, with appropriate boundary conditions:

(1) Embedded fibre end bonded

$$\begin{aligned} \sigma_f &= \sigma_{f0} \quad \text{at } z = 0 \\ \sigma_f &= \sigma_0 \quad \text{at } z = l \end{aligned} \tag{13}$$

(2) Embedded fibre end debonded

$$\begin{aligned} \sigma_f &= 0 \quad \text{at } z = 0 \\ \sigma_f &= \sigma_0 \quad \text{at } z = l \end{aligned} \tag{14}$$

2.1. Case 1

σ_{f0} is the stress in the fibre at its embedded end and satisfies the continuity condition for strains

$$\frac{\sigma_{f0}}{E_f} = \frac{\sigma_{m0}}{E_m} \tag{15}$$

where σ_{m0} is the corresponding stress in the matrix and E_f and E_m are the moduli of the fibre and matrix, respectively. The use of Equation 15 and St. Venant's principle through the equilibrium condition gives

$$\sigma_{f0} = \frac{\sigma_0}{[1 + \Phi\varepsilon]} \tag{16}$$

Solution of Equation 11, subject to Equation 13 and 16 yields the axial stress distribution in the fibre to be

$$\sigma_f = \sigma_0\frac{[1 + \Phi\varepsilon\sinh(mz)/\sinh(ml)]}{[1 + \Phi\varepsilon]} \tag{17}$$

from which the interfacial shear stress distribution along the fibre length can be derived as

$$\tau = -\frac{\sigma_0 am\Phi\varepsilon\cosh(mz)}{2[1 + \Phi\varepsilon]\sinh(ml)} \tag{18}$$

2.2. Case 2

For the case of the embedded fibre end being free, the solution of Equation 11 subject to Equation 14 leads to the set of equations

$$\sigma_f = \frac{\sigma_0}{1 + \Phi\varepsilon} \times\left[1 + \frac{\Phi\varepsilon\sinh(mz) - \sinh\{m(l - z)\}}{\sinh(ml)}\right] \tag{19}$$

and

$$\tau = -\frac{\sigma_0 am[\Phi\varepsilon\cosh(mz) + \cosh\{m(l - z)\}]}{2[1 + \Phi\varepsilon]\sinh(ml)} \tag{20}$$

2.3. Effects on stress transfer

The effect of bonding of the embedded end of the fibre ($z = 0$) on the normalized axial stress in the fibre, σ_f/σ_0 and the normalized interfacial shear stress, τ/σ_0, is shown as a function of axial position, z/l, Figs 3 and 4, respectively. The composite system used represents one with a 4% fibre volume fraction, $\varepsilon = 0.125$, and $l/a = 10$. Case 1 shows a higher axial stress in the fibre due to more effective stress transfer when the embedded fibre end is bonded. In concurrence with this, the interfacial shear stress is higher in the debonded case. It is interesting to note that the minimum value of the interfacial shear stress in the debonded case does not occur at the fibre end, but along its length. This effect is explained in the next section. An increase in ε results in less effective stress transfer (Figs 5 and 6, $l/a = 10$, $V_f = 4\%$). The axial stress at the embedded fibre end increases with a decrease in ε (i.e., an increase in fibre modulus, or a decrease in matrix modulus). The effects of aspect ratio and fibre volume fraction on the normalized axial stress are depicted in Figs 7 and 8, respectively. For both, the system used had a ratio of matrix to fibre moduli of 0.125, and results of only case 1 are shown. A change in the aspect ratio (or effectively, in the embedded length of the fibre) does not affect the value of the axial stress at the embedded end, but does affect the rate of stress transfer with the stress distribution being more uniform over a larger fibre length as the

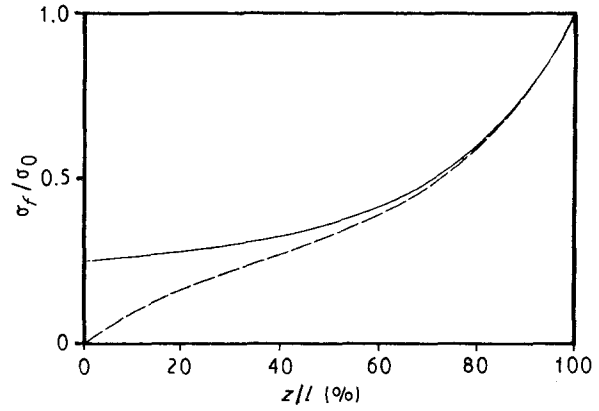

Figure 3 Normalized axial stress as a function of normalized axial position: (—) Case 1; (– – –) Case 2.

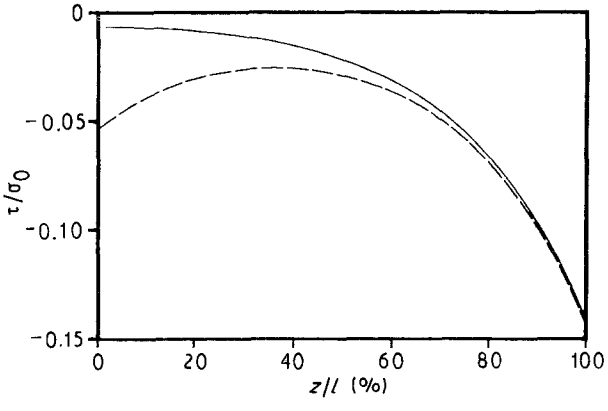

Figure 4 Normalized shear stress as a function of normalized axial position; key as Fig. 3.

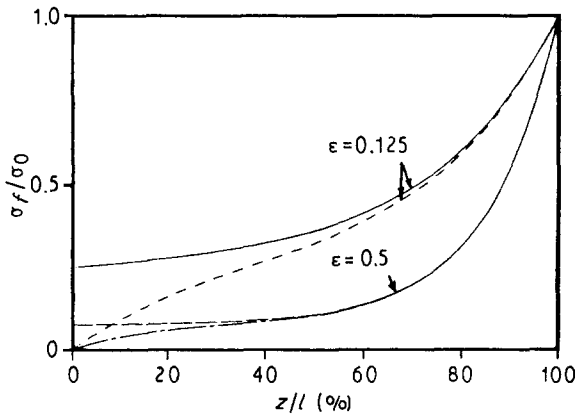

Figure 5 Effect of modulus ratio ($\varepsilon = E_m/E_f$) on axial stress in the fibre: (—) Case 1; (– – –) Case 2; (- -) Case 3 and (– - –) Case 4.

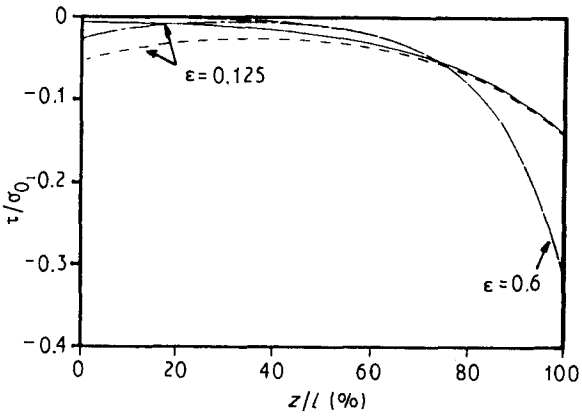

Figure 6 Effect of modulus ratio ($\varepsilon = E_m/E_f$) on shear stress; key as Fig. 4.

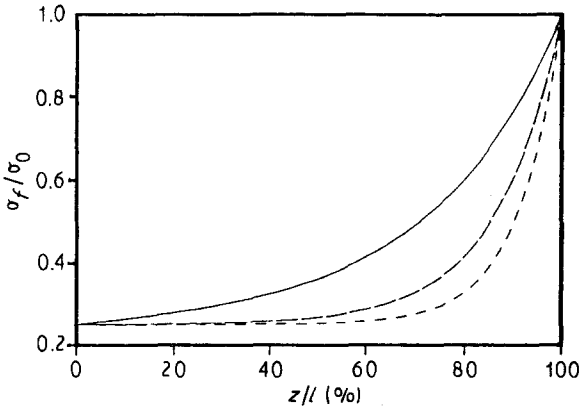

Figure 7 Effect of fibre aspect ratio on axial stress in the fibre: (—) $l/a = 10$; (– – –) $l/a = 20$ and (- -) $l/a = 30$.

embedded length increases. As aspect ratio increases, the sensitivity of the axial stress to it decreases close to the embedded end. Higher fibre volume fractions result in an increase in the axial stress along the fibre.

2.4. Effect of packing arrangement

One of the foremost challenges in the modelling of composite micromechanical behaviour is the establishment of a representative volume element (RVE). As mentioned earlier, the effect of fibre packing in the composite can be approximated through a hexagonal

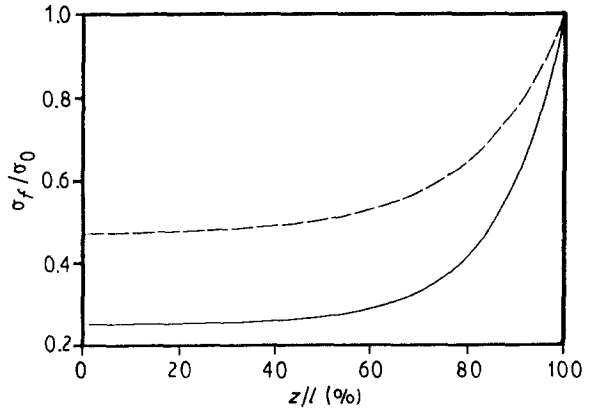

Figure 8 Effect of fibre volume fraction on normalized axial stress in the fibre as a function of normalized axial position: (—) $V_f = 4\%$ and (– – –) $V_f = 10\%$

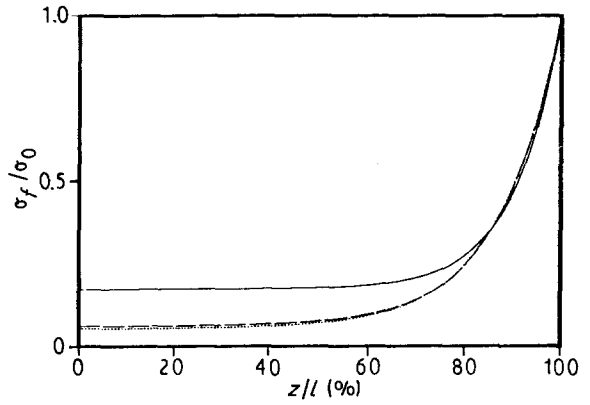

Figure 9 Effect of packing geometry on the development of fibre stress, as outlined in Section 2.4.

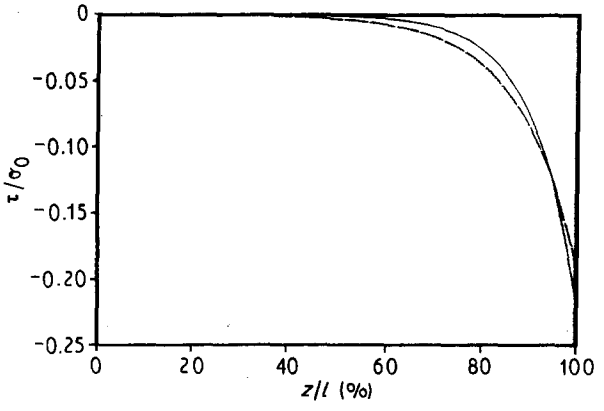

Figure 10 Effect of packing geometry on normalized shear stress as a function of normalized axial position along the fibre, as outlined in Section 2.4.

or square packing geometry. Figs 9 and 10 show the effect of packing geometry on the axial fibre stress and interfacial shear stress as a function of axial position ($V_f = 5\%$, $l/a = 20$, $\varepsilon = 0.25$). In the figure, the solid line depicts the unmodified system, whereas (–) and (. . .) represent the system as modified for square and hexagonal packing arrangements, respectively, as defined by Equation 5. The incorporation of the packing arrangement tends to lower the axial stress level, reflecting the interaction factor of fibres in the matrix, within an RVE. It can be shown that the difference in stress levels between the two different packing geometries is negligible.

3. Initiation of debonding

Debonding of the interface initiates when the shear stress at a point along the fibre–matrix interface exceeds the interfacial shear strength, τ_s. It is easily seen that for the bonded fibre end, the maximum shear stress occurs at the surface where the fibre enters the matrix. There may be some doubt in the unbonded case (e.g., Fig. 4) but it can be shown that the shear stress at the surface is always greater than that at the embedded end by considering the term

$$\Phi\varepsilon \cosh(mz) + \cosh\{m(l - z)\}$$

in Equation 20. The shear stress can be expressed as,

$$\tau \sim \Phi\varepsilon \cosh(ml) + 1 \tag{21}$$

$$\tau \sim \Phi\varepsilon + \cosh(ml) \tag{22}$$

at the surface ($z = 1$), and at the embedded end ($z = 0$), respectively. On comparison it can be seen that for an infinitely long fibre, the shear stress would always be equal at both ends and hence debonding would initiate from both the surface and embedded ends simultaneously. This would have an apparent effect on fracture toughness, which till now has been neglected. However for small embedded lengths, the stress from Equation 21 is always greater than that as computed from Equation 22, showing that in both cases debond initiation begins at the surface. The applied stress required to cause debonding, σ^*, can then be represented as

$$\sigma_1^* = -\frac{2\tau_s[1 + \Phi\varepsilon]}{am\Phi\varepsilon}\tanh(ml) \tag{23}$$

$$\sigma_2^* = -\frac{2\tau_s[1 + \Phi\varepsilon]\sinh(ml)}{am[\Phi\varepsilon \cosh(ml) + 1]} \tag{24}$$

where the subscripts 1 and 2 signify the bonded and debonded embedded fibre end cases, respectively. It is clear that the stress needed to initiate debonding in a fibre bonded at the embedded end is greater than that for one with a debonded end as

$$\frac{\sigma_1^*}{\sigma_2^*} = \frac{\Phi\varepsilon \cosh(ml) + 1}{\Phi\varepsilon \cosh(ml)} > 1 \tag{25}$$

For an infinitely long fibre $\sigma_1^* = \sigma_2^*$ in the limit.

$|\sigma_1^*/\tau_s|$, (from Equation 23), increases with V_f, but is largely independent of the embedded length of the fibre. Since the initiation of debonding signifies the first damage event, it is essential that this phase be investigated closely, both analytically and experimentally. A point of concern is whether the failure of the interface, following initial debonding, occurs due to the actual propagation of the crack face, or through plastic yielding of the matrix. Unfortunately models such as the present one are incapable of resolving this question. The variation of the ratio of debond initiating stresses for the bonded and unbonded fibre end cases, as functions of ε and V_f, is shown in Figs 11 and 12, for three lengths of fibre embedment. The fibre radius was taken as 4 μm in each case.

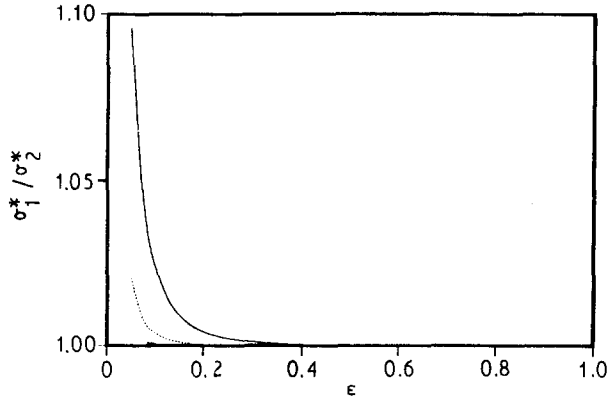

Figure 11 Effect of fibre aspect ratio as a function of modulus ratio on σ_1^*/σ_2^*: (—) $l/a = 10$; (. . .) $l/a = 15$ and (– – –) $l/a = 20$.

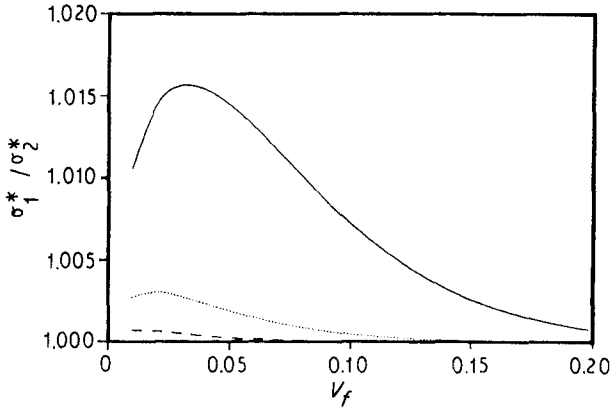

Figure 12 Effect of fibre aspect ratio as a function of fibre volume fraction on σ_1^*/σ_2^*; key as Fig. 11.

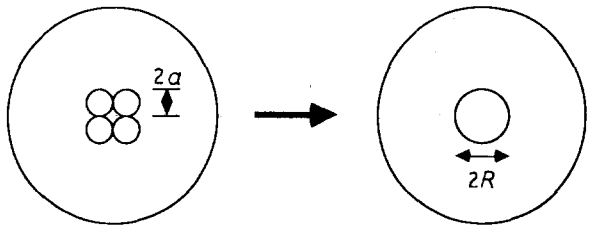

Figure 13 Equivalent bundle cross-section.

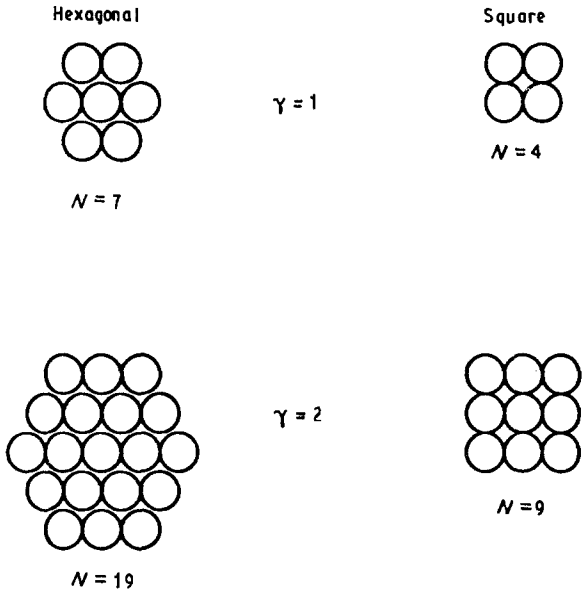

Figure 14 Packing geometries for hexagonal and square arrays.

4. Application to fibre bundles

So far we have considered a single filament enclosed within a matrix sheath. The formation of fibre bundles, or the use of tows, reduces the surface area in contact with the matrix and the reinforcing capacity of fibres is not completely utilized. For simplicity, we will curtail the discussion to bundles with hexagonal or square packing of fibres. The exposed surface area is considerably less than the actual sum of surface areas, and the equivalent radius, R, can be determined by considering an equivalence as depicted in Fig. 13.

For a bundle containing N fibres, the equivalent cross-section is given by

$$\pi R^2 = \frac{N\pi a^2}{V_b} \tag{26}$$

where a is the radius of a single filament and V_b is the packing volume fraction. $V_{b\max} = 0.907$ (erronously given as 0.912 in [19]) for hexagonal packing and 0.785 for square packing. The equivalent radius is then given as

$$R = a\left(\frac{N}{V_b}\right)^{1/2} \tag{27}$$

The number of fibres within a bundle using these two packings can be computed as

$$\begin{aligned} N &= 2\left[\gamma^2 + \frac{\gamma(\gamma+1)}{2}\right] + (2\gamma+1) \\ &= (\gamma+1)^2 \end{aligned} \tag{28}$$

for a hexagonal and square array, respectively. $\gamma = 1, \ldots, n$ and $(\gamma + 1)$ represents the number of filaments needed to form a side of the geometrical arrangement (Fig. 14). It should be noted that these are for maximum packing, and for arrangements at less than optimal, different values of V_b and N may be applicable based on the actual arrangement. The surface area of N fibres is $2\pi aN$, but since the reinforcement is in the form of a bundle, with exposed area of filaments being semicircular, the actual surface area can be computed as the product of the circumference of an equivalent cylinder of radius R and the ratio of the exposed area of a single filament ($= \pi a$, as it is semicircular) to its diameter.

$$\begin{aligned} \text{Bundle Surface Area} &= 2\pi R\frac{\pi a}{2a} \\ &= \pi^2 R \end{aligned} \tag{29}$$

Force equilibrium then gives

$$\frac{d\sigma_B}{dz} = -\frac{\pi\tau_B}{R} \tag{30}$$

where σ_B is the stress in the bundle, and τ_B is the shear stress acting at the bundle–matrix interface. A procedure similar to that in Section 2 for the derivation of the constitutive equation can be followed. For the bonded end case, the axial stress in the fibre bundle is given by

$$\sigma_B = \frac{\sigma_{0B}[1 + \Phi\varepsilon \sinh(\kappa z)/\sinh(\kappa l)]}{[1 + \Phi\varepsilon]} \tag{31}$$

where σ_{0B} is the externally applied stress on the bundle. We assume as an approximation that there is no slip within the bundle and that the axial displacement in the reinforcement core does not vary with radial distance

$$\kappa = \left\{ \frac{\pi[1 + \Phi\varepsilon]}{2(1 + \nu_m)\left[b^2 \ln(b/R) - \frac{b^2 - R^2}{2} \right]} \right\}^{1/2} \quad (32)$$

which on comparison with Equation 12 results in

$$\kappa = m\left\{ \frac{\pi V_b}{2N} \right\}^{1/2} \quad (33)$$

for the same composite volume fraction, i.e.,

$$V_f = \left(\frac{a}{b_f} \right)^2 = \left(\frac{R}{b_B} \right)^2$$

where b_f and b_B are the radii of the respective matrix sheaths. From Equations 30 and 31 the shear stress distribution can be determined as

$$\tau_B = - \frac{R\kappa\sigma_{0B}\Phi\varepsilon \cosh(\kappa z)}{\pi[1 + \Phi\varepsilon] \sinh(\kappa l)} \quad (34)$$

Figs 15 and 16 show the effect of bundle size on the normalized axial fibre stress and shear stress, respectively, as a function of the axial position along the fibre. The square packing geometry was chosen with an optimal volume fraction within the bundle of 0.785. For each bundle size the ratio l/R, where l is the embedded length of the bundle and R the equivalent bundle radius (Equation 25) was constant (= 20). Each filament/fibril within the bundle was of 4 μm radius, with the composite fibre volume fraction being 5% and $\varepsilon = 0.125$. The shear stress developed at the bundle surface is seen to be the highest for the smallest bundle ($N = 4$) at the matrix crack surface. This however is reversed away from the surface, with the largest bundle having the highest shear stress after about 40% of the fibre length from the surface. The difference in the shear stress distribution along the fibre length between the case of a single fibre (Fig. 4) and that of a bundle (Fig. 16) is clearly apparent with the shear stresses being much lower in the case of bundles,

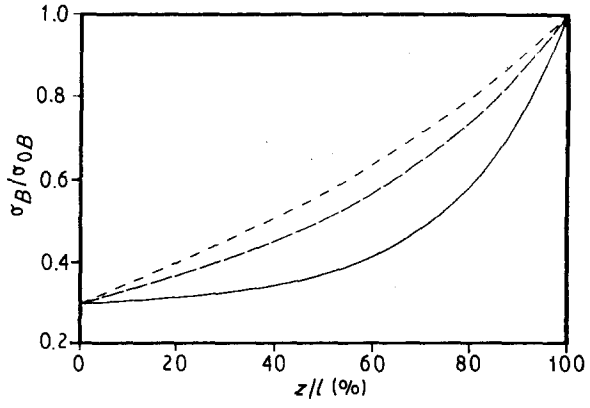

Figure 15 Effect of bundle size on the normalized axial stress in the bundle as a function of normalized axial position: (—) $N = 4$; (– – –) $N = 16$ and (– – –) $N = 36$.

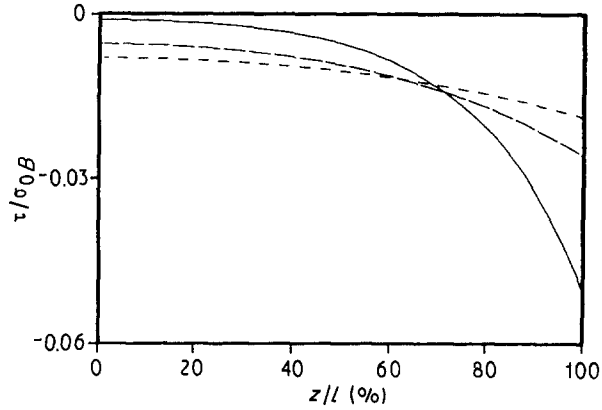

Figure 16 Effect of bundle size on the normalized shear stress in the bundle as a function of normalized axial position; key as Fig. 15.

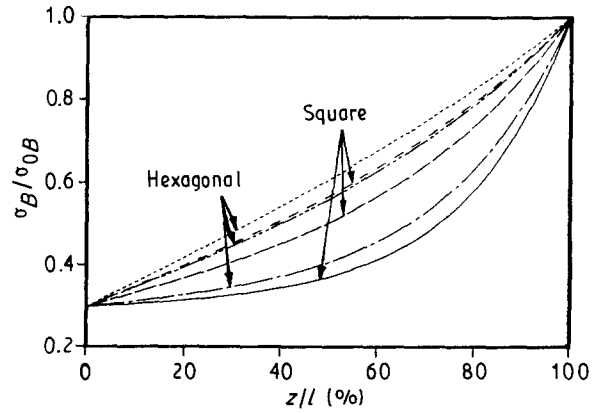

Figure 17 Effect of packing geometry and number of fibres: (—) $N = 4$; (– – –) $N = 16$; (– – –) $N = 36$; (— — —) $N = 7$; (— — — —) $N = 37$ and (. . . .) $N = 91$.

irrespective of size. A comparison of the effect of hexagonal and square packing within bundles for the same l/R ratio (= 20) can be made from Fig. 17. The square arrangement results in arrangements of 4, 16 and 36 filaments, whereas the hexagonal results in 7, 37 and 91.

As is apparent, the effectiveness of load transfer to the matrix depends on the equivalent radius, R, rather than on the number of fibres within a bundle, or the total area of fibres, ($= N\pi a^2$), included within. The number of fibres within a bundle and the equivalent radius assuming optimal packing are provided in Table 1 in the order of effectiveness of stress transfer to the matrix. Each filament was taken to be 4 μm in radius. There is very little difference between the reinforcing capabilities of the hexagonal and square packed bundles having a similar number of fibres, in spite of the difference in packing fractions, as shown for the cases of 36 and 37 fibrils in the square and hexagonal arrangements, respectively, Debonding initiation will occur at

$$\sigma^*_{0B} = - \frac{\pi\tau_{Bs}[1 + \Phi\varepsilon] \tanh(\kappa l)}{R\kappa\Phi\varepsilon} \quad (35)$$

where τ_{Bs} is the shear strength of the bundle–matrix interface. It would be of interest, for materials design, to relate and compare the debond initiating stress for a bundle with that of a single fibre through Equations

TABLE I Details of packing geometry

Packing geometry	No. of fibrils	Equivalent radius (μm)
Square	4	9.03
Hexagonal	7	11.08
Square	16	18.06
Hexagonal	37	25.48
Square	36	27.09
Hexagonal	91	39.96

23, 24 and 35.

$$\frac{\sigma_{0B}^{*}}{\sigma_{1}^{*}} = \left(\frac{\tau_{Bs}}{\tau_s}\right)\frac{\tanh\left[ml\left(\frac{\pi V_b}{2N}\right)^{1/2}\right]}{(2/\pi)^{1/2}\tanh(ml)} \quad (36)$$

Knowing the values of shear strength for the bundle and filament, the debonding stresses may be computed (or vice-versa).

5. Consideration of frictional stress

When the load applied to the fibre is such that the maximum interfacial shear stress is equal to the shear strength of the fibre–matrix interface, debonding occurs. This results in energy dissipation due to fibre–matrix sliding and a local increase in the elastic strain energy of neighbouring fibres. The term debonding relates to the stage of damage wherein there is a relative slip between the fibre and the surrounding matrix as a result of the applied load. This however does not mean that the system has failed. Some load transfer is still possible between the fibre and matrix in the debonded zone due to frictional stresses. The interfacial shear stresses will however continue to act as before along the embedded length of the fibre. The system under consideration can now be assumed to be divided into two regions as in Fig. 18. This configuration will be used to study the partially debonded fibre–matrix configuration. Following [5, 6] we consider a shear stress, τ, to act outside the debonded region and a purely frictional interfacial stress, f, to act within the debonded portion.

σ' is the stress in the fibre at the point where the two sections, debonded and perfectly bonded, meet. The difference between the stresses σ_0 and σ' is given by [15]

$$\sigma' = \sigma_0 + \frac{2f(l - z)}{a} \quad (37)$$

At the new position of the crack front, $\tau_{max} = \tau_s$ and from Equation 18 for the new configuration

$$\sigma' = -\frac{2\tau_s[1 + \Phi\varepsilon]}{am\Phi E}\tanh(mz) \quad (38)$$

From Equations 37 and 38

$$\sigma_0 = -\frac{2\tau_s[1 + \Phi\varepsilon]}{am\Phi\varepsilon}\tanh(mz) - \frac{2f(l - z)}{a} \quad (39)$$

where z represents the bonded length of the fibre.

It is intuitively obvious that the ratio of the interfacial shear strength to the interfacial frictional stress,

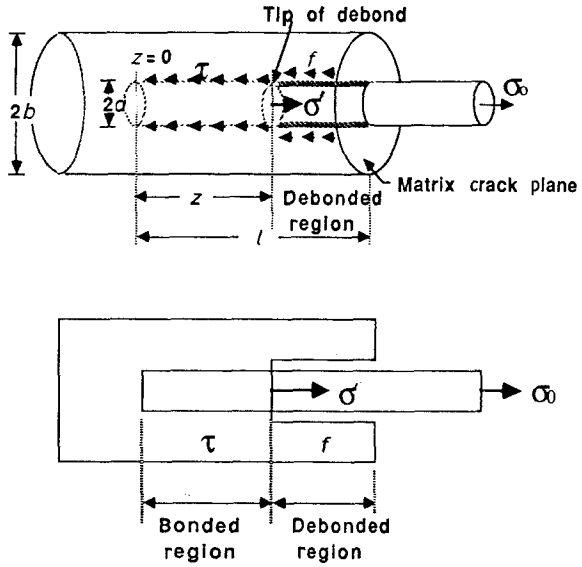

Figure 18 Schematic of shear-lag model representation of partial debonding.

as well as factors such as the remaining embedded length, the fibre volume fraction and the ratio of moduli will have an influence on whether the initial debonding will be catastrophic, or whether additional external load is required to continue the process. It is important that the stress in the fibre be less than the fibre strength, otherwise fibre fracture will result before further debonding.

In order to investigate this further, consider

$$\frac{d}{dz}(\sigma_0) = -\frac{2\tau_s[1 + \Phi\varepsilon]}{a\Phi\varepsilon}\operatorname{sech}^2(mz) + \frac{2f}{a}$$

For the extremum distance z,

$$\operatorname{sech}^2(mz) = \frac{f}{\tau_s}\frac{\Phi\varepsilon}{[1 + \Phi\varepsilon]}$$

giving

$$z_{max} = \frac{1}{m}\cosh^{-1}\left(\frac{\tau_s}{f}\frac{[1 + \Phi\varepsilon]}{\Phi\varepsilon}\right)^{1/2} \quad (40)$$

At this stage, ($l = z_{max}$), debonding is catastrophic and needs no increase in applied stress. If the embedded fibre length is greater than z_{max}, debonding will stop after the initial amount and further externally applied stress is needed to continue the process. The factors of dependence are given as

$$\frac{\tau_s}{f}\frac{[1 + \Phi\varepsilon]}{\Phi\varepsilon} = \Psi$$

When $\Psi \geq \cosh^2(ml)$, $z_{max} = l$ and debonding is instantaneous. Using this, the stress needed to get complete debonding followed by pull-out can be expressed using Equations 18 and 39, when $\tau = \tau_s$ with the above condition

$$\sigma_0^{max} = -\frac{2\tau_s[1 + \Phi\varepsilon]}{am\Phi\varepsilon}\tanh(ml) \quad l \leq z_{max}$$

$$\sigma_0^{max} = -\frac{2\tau_s[1 + \Phi\varepsilon]}{am\Phi\varepsilon}\tanh(mz_{max}) - \frac{2f(l - z_{max})}{a} \quad l > z_{max} \quad (41)$$

The case where $l \leq z_{max}$, translates as being equivalent to the expression derived by Greszczuk [4], without consideration of the interfacial frictional stress. The stress condition for interfacial failure was given as

$$\sigma_0 = -\left(\frac{2\tau}{a\alpha}\right)\tanh(\alpha l)$$

where

$$\alpha = \left\{\frac{4\pi G_m}{\ln(b/a)aE_f}\right\}$$

The parameters α from [4] and m from the present theory however differ due to the consideration of mechanical equilibrium at the embedded end of the fibre in the present case. The present theory is hence seen to be of a more general nature than that prescribed in [4], which is a special case of this theory.

For a very long fibre, $\tanh(ml) \simeq 1$, in Equation 23 and we can define the maximum stress in a very long fibre as

$$(\sigma_0^l)^{max} = -\frac{2\tau_s[1 + \Phi\varepsilon]}{am\Phi\varepsilon} \quad (42)$$

and use it to normalize the expressions for pull-out stress in Equation 39 as

$$\frac{\sigma_0^{max}}{(\sigma_0^l)^{max}} = \tanh(ml) \qquad l \leq z_{max}$$

$$= \tanh(mz_{max}) + \left(\frac{f}{\tau_s}\right)\frac{m\Phi\varepsilon}{[1 + \Phi\varepsilon]} \times (l - z_{max}) \qquad l > z_{max} \quad (43)$$

It is to be noted that $(\sigma_0^l)^{max}$ is the stress required for the complete debonding of a long fibre, resulting in the immediate catastrophic failure of the interfacial bond with no frictional stress. As can be seen from Equation 39, the effect of incorporating the frictional shear stress, f, is to increase the axial stress needed for pull-out. This again shows the toughening mechanism effect caused by the increased work of pull-out.

Nondimensionalized pull-out stress $\sigma_0^{max}/(\sigma_0^l)^{max}$ is plotted against the embedded fibre length factor, ml, for various values of τ_s/f in Fig. 19. For this plot $a^2/b^2 = 0.3$, (representing a fibre volume fraction of 0.3) $E_f/E_m = 2.0$ and a, the fibre radius was taken as 10 μm. Stress required for pull-out increases as the frictional shear stress increases, as i.e., $\tau_s/f \to 1$, whereas as $f \to 0$, i.e., $\tau_s/f \to \infty$ and all embedded fibre lengths are less than critical, the maximum pull-out load becomes independent of embedded lengths at long embedment lengths. At intermediate values, $l < \tau_s/f < \infty$, the pull-out stress versus the embedded fibre length factor curves show a point of discontinuity at $z = z_{max}$, where the slope of the curve becomes constant. This point denotes the onset of action of the frictional shear stress in addition to the interfacial shear stress.

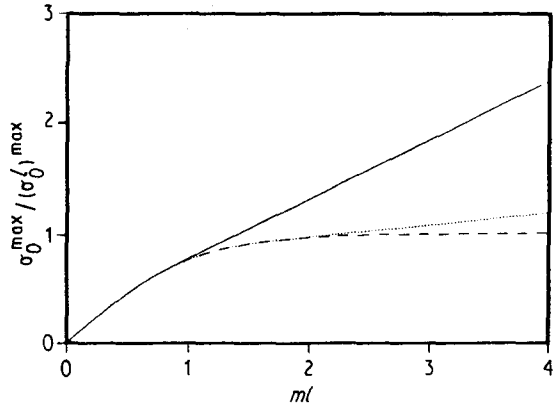

Figure 19 Normalized pull-out stress as a function of embedded fibre length factor: (—) 1; (– – –) 10 and (– – –) 100.

6. Discussion and conclusions

The effects of the scale of the constituents of a composite, and their elastic properties on the elastic load transfer, development of shear stress, debond initiation stress, and pull-out stress have been analysed in the previous sections. The end condition of the embedded fibre was varied so as to investigate the differences in load transfer and debond initiation, under the action of tensile loading in the direction of the fibre axis. The interaction effect of neighbouring fibres is built into the shear-lag model through the use of a suitable RVE describing the packing arrangement of fibres in the composite. Both square and hexagonal packings are investigated in the analysis. In reality it would be necessary to scale both the fibre and the interphase dimensions so as to match their respective volume fractions in the composite. However, due to the difficulty in characterizing the interphase, it is simply viewed as a dimensionless separation between the fibre and matrix. The effect of fibre bundling is also investigated. Stresses developed through the use of different sizes and arrangements of fibre bundles (or bundles of fibrils) are compared, as well as comparisons made of the effects of bundles as against those due to the stress being applied to a single fibril. It is determined that the shear stresses developed on the bundle surface are much lower than those developed on the interface between a single fibre and matrix. It would appear that the use of bundles is advantageous as compared to single fibre reinforcement. However, the statistics of fibril strength need to be kept in mind, in that individual fibrils within a bundle could fracture causing a telescopic type of pull-out. This could lead to lower energy absorption levels, and thereby negate the expected and desired effect of increased energy absorption through the use of reinforcement bundles. The success of braiding in the fabrication of preforms, suggests that similar techniques could be applied to the formation of bundles. There exists very little work in the area of bundle effects although this would seem to appear as a necessary investigation towards the optimal use of reinforcement and in materials design.

Both interfacial shear strength and frictional stresses are incorporated in the analysis of pull-out. The maximum applied stress necessary to cause complete debonding and subsequent pull-out is shown to be dependent on the embedded fibre length, through the definition of a critical length for catastrophic debonding, and on the ratio between the shear strength of the interface and the frictional stress present after

debonding. It was not possible to make a direct comparison between the predictions from the present theory and the results of Takaku and Arridge [7], for the pull-out of stainless steel wire embedded in epoxy, due to their experimental set-up being considerably different from the one modelled herein. In their experiment, the embedded fibre was extended to the edge of the far side of the matrix block, which is incompatible with the assumption of continuity of strains used herein. However, using their data, values of τ were computed from test results over the range of embedded fibre lengths and the overall trend for interfacial shear stress was extrapolated to $l = 0$, to get a value of τ_{max} for the system. The results are in qualitative agreement with the experimental conclusion that the interfacial shear stress generated between the clean stainless steel wire and the epoxy resin is greater than that between the mould release agent coated wire and the same resin system. The predictions for shear strength from the current theory are higher than those cited in [7] due to the aforementioned difference in set-up.

Goettler and Faber [29] used the single fibre pull-out test to measure the interfacial properties of SiC fibres in soda-borosilicate glass matrices. They reported an interfacial shear stress of 28.65 MPa for initial debonding of SCS–6 coated SiC, which was arrived at using Greszczuk's analysis. Using the present analysis a value of 29.57 MPa was arrived at. Although the difference in values is minor it is to be noted that the boundary condition at the embedded end of the fibre in the present analysis more closely replicates the actual situation.

The level of stress required to cause intermediate (non-catastrophic) debonding of length $(l - z)$ (see Fig. 18), is given by Equation 39. This relates to the case when the applied stress is just sufficient to cause debonding of the specified length, but would need a further increase in externally applied stress for the debonding to continue. It would be of interest to compare this with the level of stress needed to cause catastrophic debonding for various debonded lengths. The nondimensional stress for intermediate debonding is given by

$$\frac{\sigma_0}{(\sigma_0^l)^{max}} = \tanh(mz) + \left(\frac{f}{\tau_s}\right) \times \frac{m\Phi\frac{E_m}{E_f}}{\left[1 + \Phi\left(\frac{E_m}{E_f}\right)\right]}(l - z) \quad (44)$$

where $(\sigma_0^l)^{max}$, the normalizing factor, is defined in Equation 42. The nondimensional stress for pull-out is then

$$\frac{\sigma_0^{max}}{(\sigma_0^l)^{max}} = \tanh(ml) \qquad l \leq z_{max}$$

$$= \tanh(mz_{max}) + \left(\frac{f}{\tau_s}\right) \frac{m\Phi\frac{E_m}{E_f}}{\left[1 + \Phi\left(\frac{E_m}{E_f}\right)\right]} \times (l - z_{max}) \qquad l > z_{max} \quad (45)$$

Properties of the SiC/soda-borosilicate glass system from [29] were used as a basis for the following theoretical investigation with the embedded length being assumed as 2 mm. Curves for the normalized stress required to cause intermediate debonding against the debonded length as a percentage of the embedded length are shown in Fig. 20, for values of $\tau_s/f = 1$, 10 and 100. The initial value of the normalized stress is that required to just initiate the first debond and it follows that at this point there is no frictional stress acting. Hence there is no difference in the values of $\sigma_0/(\sigma_0^l)^{max}$ at initiation, and the value of stress required for a fibre of specified embedded length is the same as that for the very long fibre. It can however be seen that as the length of the debond, $(l - z)$, increases, stress required for intermediate debonding increases with an increase in the value of the frictional shear stress, f. In order to understand the effect of fibre diameter, plots are drawn in Fig. 21 for radii of 60, 70 and 80 μm, with $\tau_s/f = 10$. It is apparent that the debonding stress is slightly higher at smaller diameters, due to the increased plastic strain associated with debonding of smaller diameter fibres. This is in agreement with the experimental conclusions of Bowling and Groves [30].

A comparison of the stress to cause intermediate debonding and that needed to cause catastrophic debonding, in systems having the same embedded fibre length, may be made from Equations 44 and

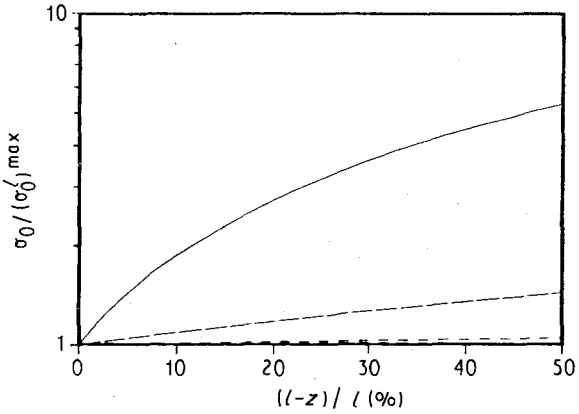

Figure 20 Normalized stress required for intermediate debonding: (—) 1; (– –) 10 and (---) 100.

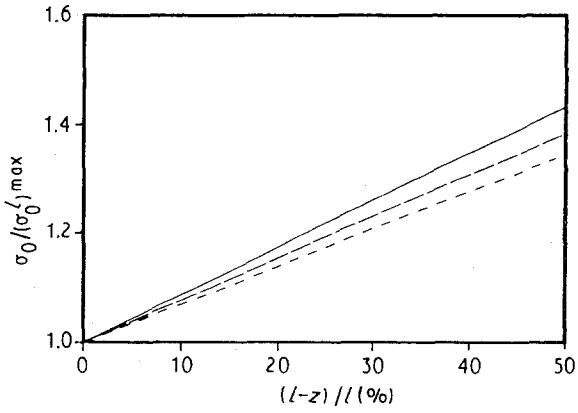

Figure 21 Effect of fibre diameter on stress for intermediate debonding: (—) 60 μm; (–) 70 μm and (– – –) 80 μm.

45 as

$$\frac{\sigma_0}{\sigma_0^{max}}$$

It can be noted that in accordance with the earlier discussion, the stress for catastrophic failure increases with the value of the frictional shear stress. Thus the values of $\sigma_0 / \sigma_0^{max}$ are lower for the higher values of frictional shear stress. On comparison it is clear that the stress needed for intermediate debonding is much less than that for catastrophic debonding when $\tau_s = f$. However, as the value of the frictional stress decreases, it is seen that there is very little difference between these stresses, especially at very low f. This clearly emphasizes the increase in toughening due to increased frictional stresses.

It is suggested that the interface properties be tailored such that the shear strength is of a value conducive to interfacial debonding as the preferred mode of damage (as against fibre breakage in the case of a very strong interface), following matrix cracking, and that the interface be such that the frictional shear stresses are as high and as close in value to the shear strength as possible. This may be achieved through coating the fibre so as to create a suitable interface which provides micro-roughness on the surface after the failure of the elastic bond. It is hoped that the present analysis will provide a firm basis for further understanding of the energetics of pull-out and the toughening mechanisms of debonding, pull-out and fibre bridging in advanced composites.

References

1. J. K. WELLS and P. W. R. BEAUMONT, *J. Mater. Sci.* **20** (1985) 1275.
2. A. G. EVANS, *J. Amer. Ceram. Soc.* **73** (1990) 187.
3. V. M. KARBHARI, J. M., HENSHAW and D. J. WILKINS, Proceedings of the 36th International SAMPE Symposium and Exhibition, San Diego, CA, April 1991 (SAMPE, 1991) p. 705.
4. L. B. GRESZCUKI, *ASTM STP* **452** (1969) 49.
5. V. M. KARBHARI and D. J. WILKINS, *Scripta Metall.* **24** (1990) 1197.
6. P. LAWRENCE, *J. Mater. Sci.* **7** (1972) 1.
7. A. TAKAKU and R. G. C. ARRIDGE, *J. Phys., D: Appl. Phys.* **6** (1973) 2038.
8. P. S. CHUA and M. R. PIGGOTT, *Composites Sci. Tech.* **22** (1985) 33.
9. Y-C, GAO, Y-W. MAI and B. COTTERELL, *ZAMP.* **39** (1988) 550.
10. A. N. GENT, G. S. FIELDING-RUSSELL, D. I. LIVINGSTON and D. W. NICHOLSON, *J. Mater. Sci.* **16** (1981) 949
11. C. GURNEY and J. HUNT, *Proc. Roy. Soc.* **A299** (1967) 508.
12. A. KELLY, *ibid.* **A319** (1970) 95.
13. J. O. OUTWATER and M. C. MURPHY, *Modern Plastics* **47** (1970) 160.
14. M. D. THOULESS and A. G. EVANS, *Acta Metall.* **36** (1988) 517.
15. J. K. WELLS and P. W. R. BEAUMONT, *J. Mater. Sci.* **17** (1982) 1275.
16. R. J. GRAY, *ibid.* **19** (1984) 861.
17. L. J. DRAZL, M. J. RICH and P. F. LLOYD, *J. Adhesion,* **16** (1983) 1.
18. C-H. HSUEH, *J. Mater. Sci.* **24** (1989) 4475.
19. A. KELLY, in Proceedings of the NPL Conference (1971) p. 5.
20. H. L., COX, *Brit. J. Appl. Phys.* **3** (1952) 72.
21. M. R. PIGGOTT, *Acta Metall.* **14** (1966) 1429.
22. Y. TERMONIA, *J. Mater. Sci.* **22** (1987) 504.
23. *Idem, ibid.* **22** (1987) 1733.
24. C. ATKINSON, J. AVILA, E. BETZ and R. E. SMELSER, *J. Mech. Phys. Solids,* **30** (1982) 97.
25. A. S. CARRARA and F. J. McGARRY, *J. Comp. Mater.* **2** (1968) 222.
26. R. A. LARDER and C. W. BEADLE, *ibid.* **10** (1976) 21.
27. E. D. REDDY, *ibid.* **18** (1984) 595.
28. V. C. NARDONE and K. M. PREWO, *Scripta Metall.* **20** (1986) 43.
29. R. W. GOETTLER and K. T. FABER, *Composites Sci. Tech.* **37** (1990) 129.
30. J. BOWLING and G. W. GROVES, *J. Mater. Sci.* **14** (1979) 431.

Received 21 August 1990
and accepted 28 February 1991